

Contents lists available at ScienceDirect

Materialia

journal homepage: www.elsevier.com/locate/mtla



Full Length Article

Twin nucleation from disconnection-dense sites between stacking fault pairs in a random defect network

Kehang Yu^a, Xin Wang^a, Subhash Mahajan^b, Irene J. Beyerlein^c, Penghui Cao^{a,d}, Timothy J. Rupert^{a,d}, Julie M. Schoenung^a, Enrique J. Lavernia^{a,*}

- ^a Department of Materials Science and Engineering, University of California, Irvine, Irvine, CA 92697, USA
- ^b Department of Materials Science and Engineering, University of California, Davis, Davis, CA 95616, USA
- Eppartment of Mechanical Engineering, Materials Department, University of California, Santa Barbara, Santa Barbara, CA 93106, USA
- ^d Department of Mechanical and Aerospace Engineering, University of California, Irvine, Irvine, CA 92697, USA

ARTICLE INFO

Keywords: Twin nucleation Pure-shuffle Stacking fault Molecular dynamics

ABSTRACT

Deformation twinning, an important plastic deformation mode, critically influences the strength and ductility of Mg. As such, a fundamental understanding of twin nucleation will provide us with an important insight into the conditions that favor the onset of this deformation mode. To reveal the twin nucleation mechanism, we construct a defect network without making assumptions about the types and relative densities of dislocations present. The generated defect network features a high density of I_1 stacking faults as well as disconnections between them. Deformation modeling results suggest that this structure enables a twin nucleation event from disconnection-dense sites between I_1 stacking faults pairs. By probing twin nucleation and early-stage growth inside of the random defect network, we propose a geometry-based twin variant selection rule as well as a pure-shuffle twin nucleation and early-stage growth mechanism underpinning twinning in Mg.

1. Introduction

Mg-rich alloys are of interest as structural materials, due to their low densities and great potential for weight savings. However, their low strength and limited formability at room temperature have led to concerns regarding reliability and manufacturability [1]. These undesirable properties are attributable to the limited number of slip modes that can be easily activated during plastic deformation and the relative ease of twinning, a unidirectional deformation mode, in hexagonal close packed (hcp) structure. Depending on the type of twin, deformation twinning can accommodate either <c>-axis contraction or extension but not both. To date, numerous studies have focused on uncovering the mechanisms that govern twin nucleation, as well as early-stage twin growth following nucleation, in hexagonal close packed metals like Mg and its alloys [2-6]. Twin nucleation typically occurs much too rapidly for direct observation via electron microscopy techniques, making it challenging to understand all of the possible ways and situations in which twins can form [7]. Therefore, there is a lack of scientific understanding on precisely how twinning occurs, and hence numerous theories and mechanisms have been proposed to explain twin nucleation

and establish the conditions that enable this event [7–14]. Most of these proposed mechanisms pertain to heterogenous nucleation or defect-assisted twin nucleation since homogenous nucleation requires stresses that can be as high as the theoretical strength of the material to be activated [15]

Most conventional defect-assisted twin nucleation theories postulate that pre-existing dislocations may undergo dissociation or recombination to generate a type of precursor structure (e.g., single- or multi-layer stacking fault) for deformation twins, which assists the development of a twin nucleus [15]. In the case of the $\{10\overline{1}2\}$ twin in Mg, multiple (instead of a single) twinning disconnections (TDs) $\frac{1}{15}\langle 10\overline{11}\rangle \{10\overline{12}\}$ are most likely to be the precursor and facilitate the twin nucleation by simultaneously gliding [8]. This type of TD-induced $\{10\overline{12}\}$ twin nucleation is also referred to as shear-shuffle mechanism [7] because the atomic displacement field during the TD-facilitated lattice reorientation contains both shear and shuffle components [15,16]. In the presence of a stress concentration, multiple TDs may form via the combination of a basal <a>slip and a pyramidal-I <c+a>slip [9], the dissociation of edge <c> and mixed <c+a> dislocations [10], or the interaction between a basal dislocation and a $\{11\overline{2}1\}$ twin [11].

E-mail address: lavernia@uci.edu (E.J. Lavernia).

^{*} Corresponding author.

The pure-shuffle twin nucleation mechanism postulates that atomic shuffling, a non-affine (i.e., the displacements cannot be completed solely by a linear transformation) and diffusionless atomic displacement, akin to that involved in martensitic transformation, causes twin nucleation. While defects are still needed for the atomic shuffling, this mechanism requires far fewer TDs, other dislocations or stacking faults to be present, if any. The shuffling-induced twin nuclei feature: (1) a basal-prismatic (BP) and prismatic-basal (PB) transition and subsequently BP and PB interfaces bounding the twin embryo, and (2) a deviation of the misorientation angle from the ideal 86.3° to approximately 90° which complies with the BP and PB transition. There are more direct observations supporting the pure-shuffle nucleation mechanism than any of the other proposed mechanisms [7,13,14,17]. In summary, the two possible twin nucleation mechanisms, the shear-shuffle mechanism featuring the nucleation of precursing $\frac{1}{15}$ $10\overline{11}$ \{10\overline{12}\} TDs via multiple possible dislocation reactions and the pure-shuffle mechanism featuring a BP or PB transformation [18], may represent mutually competing pathways that lead to the formation of twins, depending on the microstructures and stress conditions that are present.

In this study, we use the following molecular dynamics (MD) simulations procedures to shed light into twin nucleation and the associated preferred twin nucleation sites, as well as into early-stage twin growth behavior. We use a random defect network that can be considered a facsimile of a real Mg sample containing a large number of crystal defects as follows. First, we construct a defect network without making assumptions of the types and relative densities of dislocations present. To build it, we employ the method introduced by F. Sansoz [19]. The generated defect network features a high density of $\rm I_1$ stacking faults as well as disconnections between them. Deformation modeling reveals that this structure enables an unusual twin nucleation event happening in disconnection-dense sites between stacking fault pairs. Second, by observing twin nucleation and early-stage twin growth inside of this system, a geometry-based twin variant selection rule and a pure-shuffle twin nucleation mechanism are proposed.

2. Computational methods

The atomic-scale mechanism responsible for $\{10\overline{1}2\}$ twin nucleation in pure Mg is investigated with the Large-scale Atomic/Molecular Massively Parallel Simulator (LAMMPS) [20], using MD with an embedded atom method (EAM) interatomic potential by Sun et al. [21]. This potential provides accurate description of dislocation core structures and stacking fault parameters [11]. To enable the twin nucleation inside bulk Mg (i.e., without the assistance of free surfaces), lattice defects like dislocations are needed to offer sites for heterogeneous nucleation [15]. Consequently, a defect network is built following the method described in Ref. [19]. This method mimics the process of dislocation formation in quenched materials with supersaturation of vacancies and no explicit assumptions of dislocation types and proportions [22]. The initial configuration is a pure Mg cube containing 963,200 atoms with dimensions of 27.40 nm along the x-direction (i.e., $[11\overline{2}0]$), 27.60 nm along the y-direction (i.e., $[\overline{1}100]$) and 28.96 nm along the z-direction (i.e., [0001]), with periodic boundary conditions applied along all three directions. After energy minimization, 20% of Mg atoms are randomly deleted from the Mg cube and a series of heat treatments is conducted under the isothermal-isobaric ensemble (NPT) ensemble with a Nosé-Hoover thermostat and a constant pressure of 0. The simulated heat treatment is schematically illustrated in Fig. 1: equilibration at 300 K for 50 ps, heating from 300 K to 823 K (i.e., 100 K below the melting temperature of Mg) over 50 ps, annealing at 823 K for 50 ps, quenching from 823 K to 1 K over 50 ps and another equilibration at 1 K for 50 ps. We select 1 K as the final temperature to minimize thermal fluctuations and enable detailed atomic analysis. By varying the random seed controlling atom removal (i.e., which 20% of atoms are to be removed) and

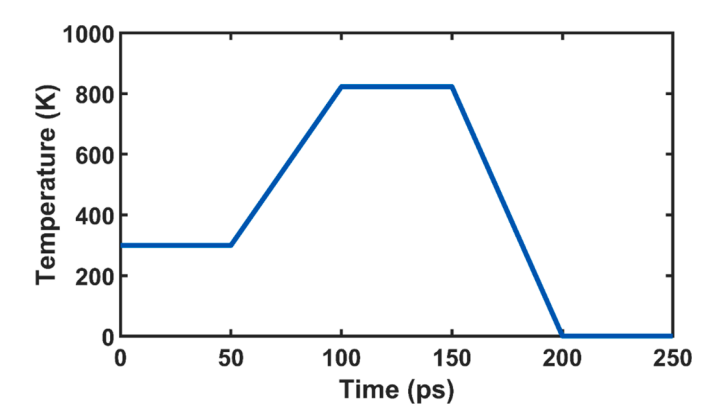


Fig. 1. Temperature and time curve in thermal annealing simulation to generate a random defect network in a Mg single crystal.

keeping other parameters consistent, we prepare four additional microstructures to validate the generality of the randomized defect network and the resulting twin nucleation mechanism.

After the heat treatment, apart from the presence of dislocations and stacking fault networks, a notable feature of the atomic arrangement is the presence of a considerable number of residual vacancies. These vacancies result from the removal of atoms before the heat treatment takes place. These are filled as best as possible with Mg atoms to minimize the effect that they may have on the twin nucleation. The Wigner-Seitz analysis [23] is done to label the vacancies and allow vacancy filling for approximately 20,000 vacancies to reduce the vacancy count to a mere 2,000–3,000. For the convenience of the readers, it is worth noting that the concentration of vacancies mentioned here is approximately 10^{-3} , which is higher compared to the equilibrium vacancy concentration of 10^{-5} at the melting temperature of Mg [24]. After that, the sample is first relaxed using energy minimization, then equilibrated using the NPT ensemble at 1 K for 250 ps and finally deformed along the z-axis at an engineering strain rate of 10^9 s⁻¹, a strain rate that is selected because it is widely used in simulating Mg deformation [11,25, 26]. The canonical (NVT) ensemble with a Nosé-Hoover thermostat is used during deformation. For all the simulations, the timestep is set to be 5 fs. The snapshots of atomic configurations in this study are all visualized by OVITO [23].

3. Results

3.1. Stacking fault network

Fig. 2(a) shows the simulation cell prior to deformation. A complex and random network of defects is generated, and the corresponding dislocation density using dislocation analysis (DXA) in OVITO [27] is estimated to be on the order of 10^{17} m⁻², which is much higher than the dislocation density of heavily deformed metals (i.e., 10^{14} - $10^{15}\ m^{-2}$) [22] and that of focused ion beam (FIB)-fabricated metallic nanopillars (i.e., $10^{15} \, \mathrm{m}^{-2}$) [19] and represents a highly defective region within a grain. The relatively high density of dislocations allows for the co-existence of dislocations with different types and lengths and is a prerequisite to enable the study of twin nucleation via MD, which is not meant to reflect physical densities that could be feasibly reached experimentally. DXA also shows the existence of almost all types of dislocations that have been frequently reported in Mg, including <a>>, <c>, <c+a>, Shockley partials (or partial <a>), Frank partials and different types of partial <c+a> slip. The random generation of high-density dislocations enables the study of the interaction between stacking faults and a disconnection-dense structure resulting from these interactions. Fig. 2(b) shows an overview of the defect network, containing plenty of I1 stacking faults shown as single-atomic-layered face-centered cubic (fcc)-type defects, relatively fewer I2 stacking

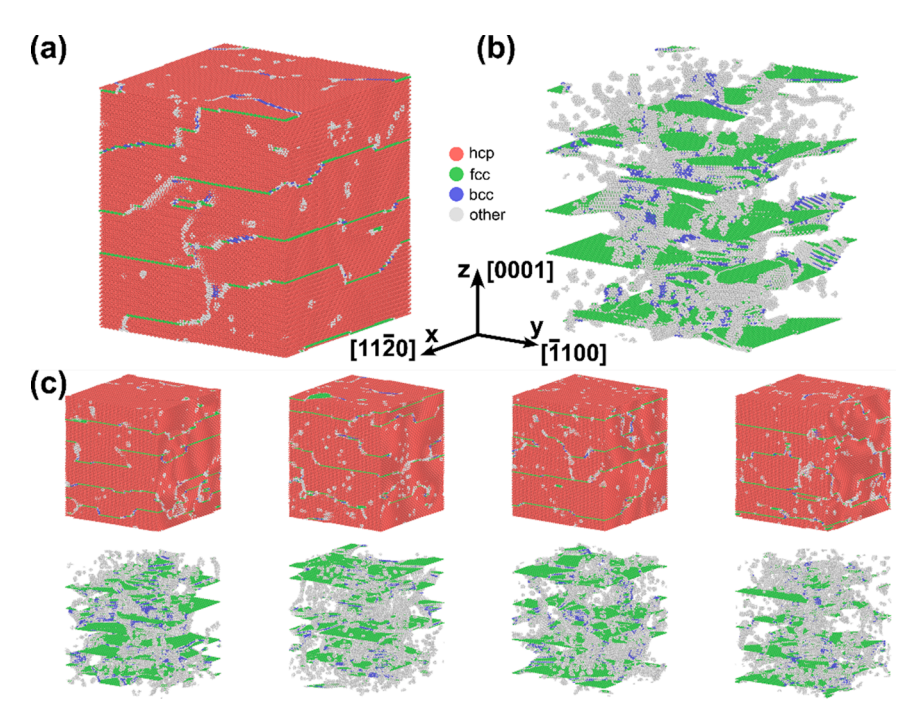


Fig. 2. Atomic snapshots before deformation (a) with hcp atoms shown, (b) without hcp atoms for clarity of the stacking fault network, (c) from the other four parallel simulations with the random seeds controlling the atom removal changed, both with (top row) and without hcp atoms (bottom row). Atoms are colored based on the polyhedral template matching algorithm in OVITO: red for hexagonal close packed (hcp), green for face-centered cubic (fcc), blue for body-centered cubic (bcc), and white for undefined local coordination structure. The color coding of atoms for the rest of this paper also follows the same rule. Tension is applied along the z-direction.

faults, pre-existing twins, and a few residual vacancies, apart from the dislocations. The most noticeable type of defects is the I₁ stacking fault that lies on the horizontal (0001) plane. The I₁ and I₂ stacking faults in the hcp system are both intrinsic stacking faults that introduce an extra half plane. The I1 stacking fault can be generated by vacancy condensation, which agrees with the formation condition in this study, and a displacement of $\frac{1}{2}\langle 10\overline{1}0\rangle$ above the vacancy. The bounding partials of an isolated I1 stacking fault then become a pair of Frank partials (i.e., $\frac{1}{6}\langle 20\overline{2}3\rangle$). On the other hand, the I₂ stacking fault can form by the direct dissociation of a basal $\langle a \rangle$ dislocation and therefore is bounded by a pair of Shockley partials (i.e., $\frac{1}{3}\langle 10\overline{1}0\rangle$) [22,28]. Fig. 2(c) shows results from the four parallel simulations which are consistent with those in Fig. 2(a) and 2(b). Unlike isolated I1 stacking faults that are bounded by Frank partials, I1 stacking faults in this model are interconnected by disconnections. A similar but much simpler configuration has been only reported by C. He et al. [29] both via experiments and simulations in a cold-rolled Mg-Bi alloy - it has been argued that a long Frank partial bounded I_1 stacking fault may interact with a basal $\langle a \rangle$ dislocation and result in a Shockley partial at the edge of a step structure connecting two I_1 stacking faults that are $\frac{1}{2}$ c (i.e., one atomic layer) spaced from each other along the c-axis. However, in this study, the step height is not limited to ½ c, while the dislocation character of the disconnection is not necessarily only one Shockley partial.

Similar to the configuration reported by C. He et al. [29], we can formulate the stacking sequence mismatch and, therefore, the formation of the ½ c-high step as shown schematically in Fig. 3(a). The Shockley partial represents the displacement of the atoms below the higher I₁ stacking fault with respect to those below the lower I1 stacking fault. If this geometry is generalized by introducing a set of Shockley partials layer-by-layer, a more complicated structure of disconnections between two I₁ stacking faults can be proposed. In Fig. 3(b), two opposite Shockley partials participate in the formation of a two-layer high disconnection. While the first Shockley partial displaces the atoms beneath the higher I1 stacking fault, the second opposing one may shift those beneath the first Shockley partial back. The overall effect is that only the stacking sequence of one layer in the middle changes from C to A. The rest of the layers are arranged the same way as if there exists no disconnection but an ideal I1 stacking fault. Similarly, multi-layer disconnections may be constructed by multiple Shockley partials, as shown

in Fig. 3(c) and 3(d). The Shockley partials are equally spaced layer-by-layer with nearest neighbors having opposite Burgers vectors. Theoretically, the arrangement of the Shockley partials can accommodate the stacking sequence mismatch between two I_1 stacking faults that are arbitrarily far away from each other while the overall Burgers vector of the disconnection is reasonably small to not further decompose.

Fig. 4 shows examples of disconnections that connect the neighboring I1 stacking faults. All the disconnections are labeled with their step heights in terms of the number of atomic layers. The two disconnection sites that later allow for twin nucleation are highlighted in orange with a circle. For given two I1 stacking faults, such as the highlighted two in Fig. 4, there are multiple ways the disconnection(s) in between can arrange themselves. A disconnection may decompose into multiple disconnections with smaller step heights. As a result, there must be a few smaller I1 stacking faults positioned in the middle to connect these decomposed disconnections with smaller step heights, as indicated by the five disconnections underscored with a dashed line compared to those marked by a solid line. On the other hand, these disconnections with larger step heights are stable because the horizontal spacing between the two bounding I₁ stacking faults is very small, usually less than 5a where a is the lattice constant of Mg, making the decomposition less likely to happen. An example with such a small horizontal spacing, which is the disconnection denoted by the orange "4" in Fig. 4, is illustrated in the inset. Interestingly, it has been found that these disconnections with larger step heights usually have a bodycentered cubic-type local atomic configuration.

3.2. Twin statistics

The analysis of twin statistics is used to characterize twin evolution quantitatively during deformation and provide insight into twin nucleation and subsequent growth. By utilizing local lattice orientation calculations in OVITO [30], it becomes possible to differentiate twins from their adjacent atoms based on quaternion differences. This capability allows for the analysis of twin-related statistics such as volume, count, variant, and shape. Twin clusters with at least 20 atoms are sorted out for twin statistical analysis. The threshold of twin size is selected so that very small atom clusters that are erroneously labeled as twins due to the instability of the algorithm will not be counted. Fig. 5 shows the twin

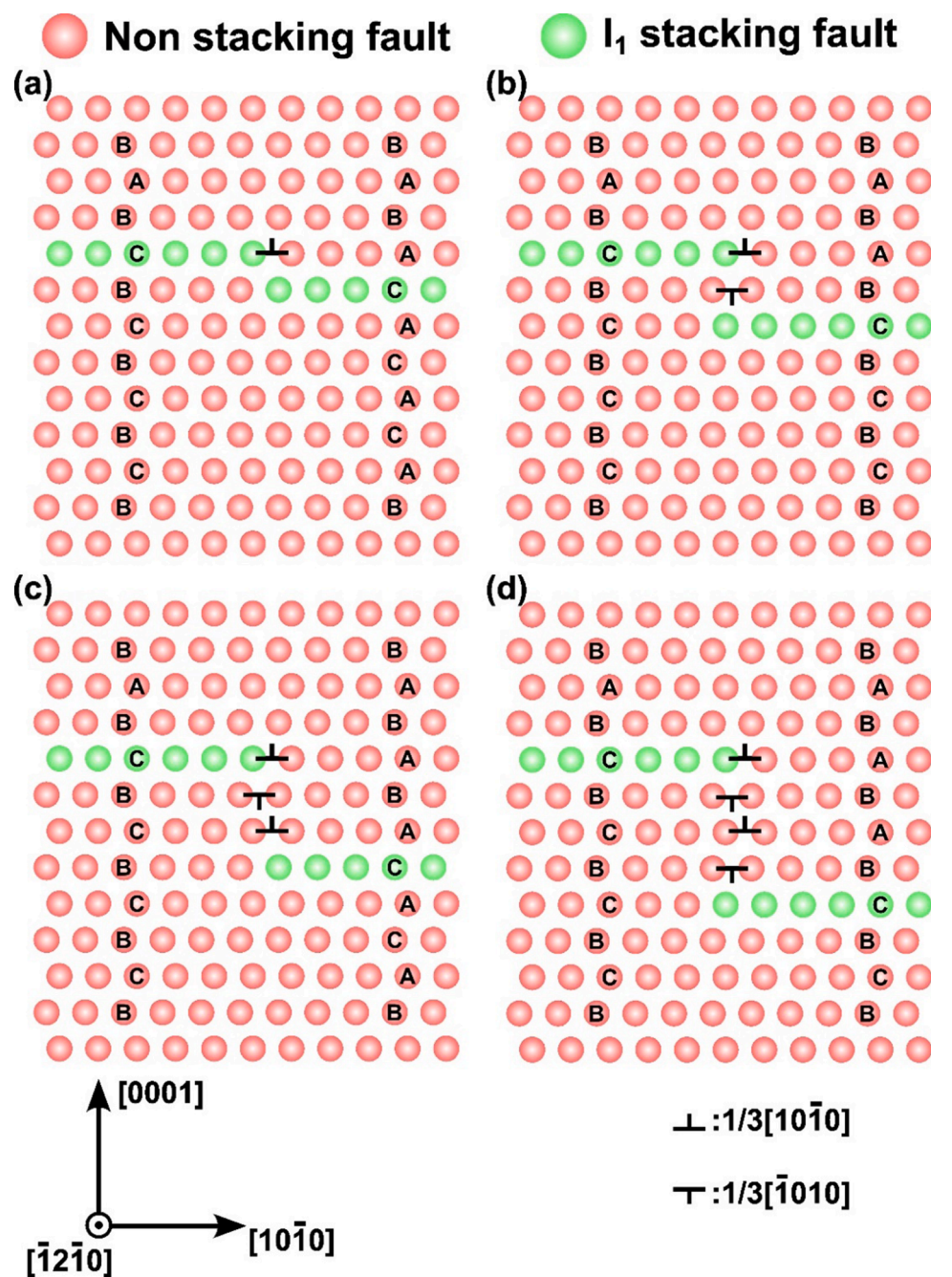


Fig. 3. A proposed formation mechanism for a (a) single-layer-high disconnection, (b) double-layer-high disconnection, (c) (2n-1)-layer-high disconnection and (d) 2n-layer-high disconnection between two bounding I_1 stacking faults. The formation is enabled by the displacement along one (for (a)) or multiple mutually opposite Shockley partials in sequence (for (b)-(d)). The Shockley partial array is also plotted as well as the resultant change in stacking sequence. Note this is a schematic diagram with unrelaxed atomic positions.

statistics using four descriptors - twin volume fraction, the number of twins, twin variant fraction, and the aspect ratio. The data are obtained from five parallel simulations with varied 20% atom deletion and slightly different defect networks. The analysis goes until an engineering tensile strain of 5%, because fracture starts to occur at larger strains.

Twin volume fraction evolution as a function of the engineering tensile strain, shown in Fig. 5(a), reveals that two different modes of twin evolution exist. One features a critical strain of ~3% after which the twin volume fraction sharply increases, like Samples 2 and 4. The other shows a less significant increase of the twin volume fraction, as in Samples 1, 3 and 5. The twin growth can be even locally reversible, as evidenced by a drop in the twin volume fraction for Sample 3, because some twin configurations are energetically unstable and therefore likely to de-twin. The disparity observed between Samples 2/4 and Samples 1/3/5 can be attributed to the stochastic nature of atom deletion and, consequently, the randomness associated with the formation of the

defect network. However, how to properly describe the randomness and correlate it to twin nucleation and early-stage growth remains an open question.

The number of twins shown in Fig. 5(b) generally increases as deformation continues. However, fluctuations in the curves indicate that changes in the number of twins result not only from nucleation, but also from twin coalescence or de-twinning. In this particular case, detwinning results from twin embryos whose subcritical size makes them unstable.

The distribution of twin variants, averaged across all samples and illustrated in Fig. 5(c), reveals an unbalanced distribution of six twin variants. Mechanically, the six variants of the $\{10\overline{1}2\}$ twin should be equally probable because the tension field was applied along the symmetry axis of the hcp crystal (c-axis). However, the observed disparity indicates that the twin variant is dictated by other structural reasons and hence that a variant selection rule may exist. Within the same twin, the

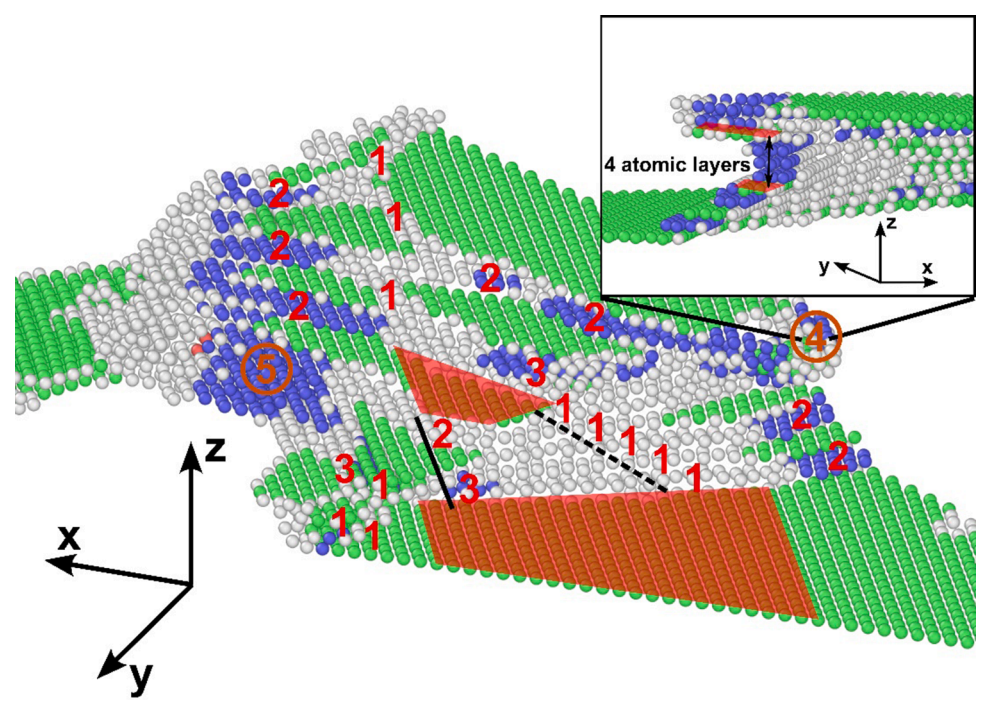


Fig. 4. The atomic snapshot of a region with dense disconnections. The step height of each disconnection is labeled in the number of atomic layers, with 1 corresponding to a height of ½ c. Numbers are colored according to whether there is a {10-12} twin nucleating at the corresponding site: orange with a circle for the nucleation site and red for the nonnucleation site. Between the highlighted two bounding I1 stacking faults, a region containing "decomposed" disconnections with lower step heights as well as smaller I1 stacking faults is marked by a dashed line, while another region containing disconnections with larger step heights is also marked by a solid line as a comparison. An enlarged view of the top-right 4 atomic-layer-high disconnection is shown in the inset with its step height and the horizontal spacing of the bounding I1 stacking faults highlighted.

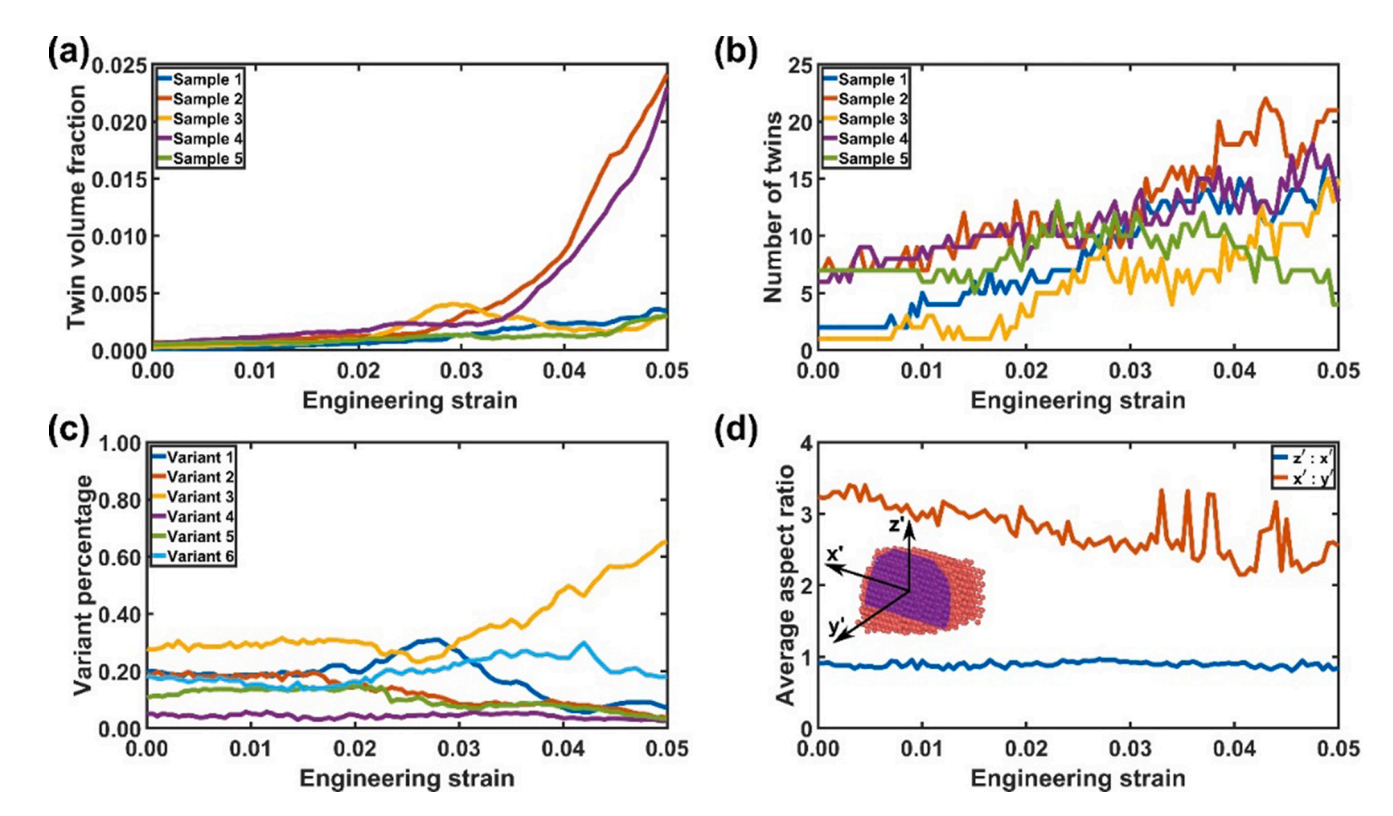


Fig. 5. (a) Twin volume fraction evolution for each sample. (b) Twin amount evolution for each sample. (c) Twin variant distribution averaged across all 5 samples. (d) Average aspect ratio evolution across all 5 samples in two ratios (z':x' and x':y') with the inset showing a local twin coordinate system and defining x'-, y'- and z'-directions: x' for the zone axis shared by the basal plane in the matrix and in the twin, y' for the in-plane perpendicular direction to the zone axis, z' for exactly the z-direction of the simulation box. All these parameters are plotted as functions of engineering strain ε_{zz} .

variant indicator can be different but only within the mutually co-zone variant pair (i.e., Variant 1-Variant 4, Variant 2-Variant 5, Variant 3-Variant 6 in Fig. 5(c)) and indicate the degeneracy of co-zone variants, which means at stages of twin nucleation and early-stage growth, co-zone twins may not be clearly distinguished. This degeneracy agrees

with a prior study by Hu et al. [31], which reveals that the twin embryo may undergo a stochastic incubation stage when co-zone twin variants are not yet determined until the twin embryo reaches a significant size in the deterministic growth stage.

The twin morphology is indicative of the nucleation mechanism as

well as the dominant growth direction of $\{10\overline{1}2\}$ twins. The twin lengths along three dimensions, the zone axis shared by the basal plane in the matrix and in the twin (labeled as x' and referred to as the zone axis hereinafter), the in-plane perpendicular direction to the zone axis (y'), and the z-axis of the simulation box (z'), of a $\{10\overline{1}2\}$ twin are shown in the inset of Fig. 5(d) and estimated using four times the standard deviation of each coordinate of atoms (i.e., their x', y' and z' values) [32]. Fig. 5(d) shows the evolution of two aspect ratios: z':x' and x':y'. The ratio z':x' is close to 1 and only slightly decreases as the applied strain increases, which implies that the growth along these two dimensions occurs concurrently and at similar rates. The ratio x':y' is always larger than 2 and generally decreases as deformation continues. This means the growth along the y'-direction is impeded relative to that along the x'- and z'-directions, especially for low strain levels. Hence, the results in Fig. 5 (d) indicate that the geometry of the twins in the system is plate-like.

3.3. Twin nucleation and early-stage growth during deformation

In what follows, we present twin statistics to provide an overview of twin evolution and therefore help in understanding a few key events during deformation. Then, the rules that may be active throughout the process of twin nucleation and early-stage growth will be discussed.

Prior to discussing these results, however, it is important to note that there are a few pre-existing $\{10\overline{1}2\}$ twins present even before deformation, although these twins are far fewer than the deformation-induced ones. These pre-existing twins are induced by the vacancy filling and the equilibration that follows because no pre-existing twins are observed in the case without these two processes. There is no significant difference in twin behavior (e.g., nucleation site, growth rules) between the pre-existing twins and the deformation-induced ones. Consequently, pre-existing twins will not be discussed separately.

In our results, twin nucleation is observed to consistently occur only at some of the disconnections between two I_1 stacking faults. A twin nucleation event is illustrated in Fig. 6 with the atom snapshots before and after the nucleation. As shown in the inset of Fig. 6(b) by four vertical basal planes in the twin, the twin embryo right after the nucleation is a 90° {1012} twin and the dominant boundary between the twin domain and the matrix is the BP/PB interface, which indicates the critical role of the P-B transformation (i.e., the prismatic plane in the matrix is transformed into the basal plane in the twin) on the twin nucleation. Notably, the formation of a coherent twin boundary is not observed during deformation. From an overview of all twin embryos, there seems to be a critical disconnection height that allows for twin nucleation. - the threshold value is four atomic layers, while the maximum height of disconnections that allows for twin nucleation is 21 atomic layers.

The unbalanced twin variant frequency has been evaluated by statistical analysis and indicates a geometrical reason behind it. Following the proposed formation mechanism of disconnections where the twin nucleation occurs, shown in Fig. 3, the edge Shockley partial also has 6 variants with 3 unique line directions due to the 6-fold symmetry of the hcp structure. By observing the nucleation of every twin embryo, the

variant selection follows simply from the geometrical constraint that for the dissociation event to occur, the zone axis must coincide with the dislocation line of edge Shockley partials. This alignment is also illustrated in Fig. 6. In other words, the 90° P-B transformation must happen on the plane spanned by the z-direction and the line direction of the disconnection in Fig. 6(a), which coincides with the x'z' plane in Fig. 6 (b), and later other parallel crystal planes. The variation in the frequency of each twin variant can be attributed to the variant selection rule, which arises from differences in the occurrence of Shockley partials along specific line directions. In other words, the frequency difference among twin variants is influenced by the presence of stacking fault pairs with specific orientations. Considering the twin morphology statistics, the P-B transformation happens faster along the x'-axis and much slower along the z'-axis, possibly due to the confinement induced by two bounding I₁ stacking faults. Also, the degeneracy of co-zone twin variants revealed by the statistical analysis is a direct consequence of the P-B transformation because the crystallographic orientation of co-zone twins will be the same after this 90° transformation.

Early-stage twin growth is defined as the significant size increase of the twin embryo that occurs immediately following twin nucleation, during which the twin size only slightly changes. Generally, the earlystage twin growth process can be divided into two substages. In the first substage, where the twin embryo grows from the state shown in Fig. 7(a) to Fig. 7(b), the transformed basal plane further expands but is still limited by two I₁ stacking faults between which the disconnection is positioned. In the meantime, the twin also grows along the y'-direction as more P-B transformations occur (denoted by three adjacent basal planes in the twin highlighted in Fig. 7(b)) but much more slowly than along the x'-direction, the zone axis. In the second substage where the state in Fig. 7(b) further evolves to that in Fig. 7(c), the twin domain will also significantly expand along the z-axis and break the limit imposed by I₁ stacking faults by reorienting the atoms in the vicinity of them. The dimensions along the three axes x', y', and z' of this twin are also shown in Fig. 7(d) under different strain levels as well as approximate boundaries of the two substages. The twin growth behavior indicates that the early-stage twin growth matches the pure-shuffle mechanism instead of the shear-shuffle mechanism, since the twin growth is still facilitated by P-B transformations and the growth along the twinning direction is not observed. It is challenging to further decompose the P-B transformation during twin nucleation and early-stage growth into meaningful finer components due to the rapid crystal shuffling.

Comparative simulations have also been done by deleting 15% Mg atoms instead of 20% while keeping all other parameters constant. Interestingly, in this case the only stacking fault type observed is the $\rm I_2$ stacking fault, which indicates the removal of abundant Mg atoms is a prerequisite to forming the $\rm I_1$ stacking fault. The $\rm I_2$ stacking fault is bounded by Shockley partials as normal and is also interconnected but by an $<\!a>$ dislocation that can be formed by the combination of two Shockley partials. When the simulation box is deformed the same way, no deformation twins are observed until sample fracture. Similarly, another comparative simulation with 18% atom deletion is conducted. In this case, $\rm I_1$ stacking faults are observed but with a smaller number

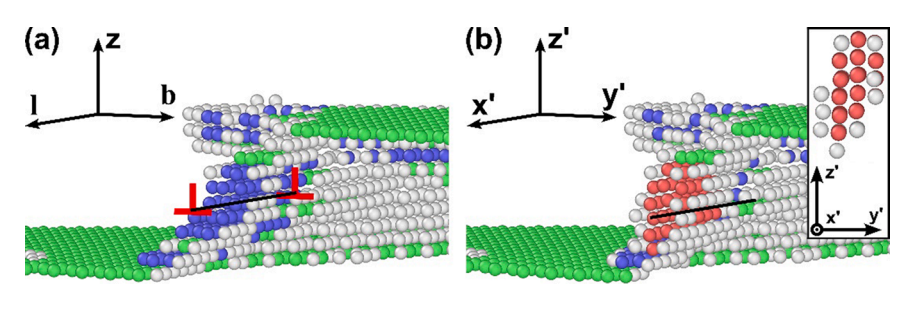


Fig. 6. Atomic snapshots of a twin nucleation site (a) right before the nucleation and (b) right after the nucleation. The inset of (b) shows this twin embryo along the x'-axis consisting of four vertical basal planes. The black lines and the coordinate systems indicate the coincidence of the dislocation line of the edge Shockley partial and the zone axis shared by the basal plane in the matrix and in the {10–12} twin embryo. The axes of the coordinate systems have the following meaning: b for the Burgers vector of the Shockley partial, 1 for the line direction of the Shockley partial, z for the z-direction of the simulation box. The x', y' and z' coordinate system has the same meaning as defined in Fig. 5(d).

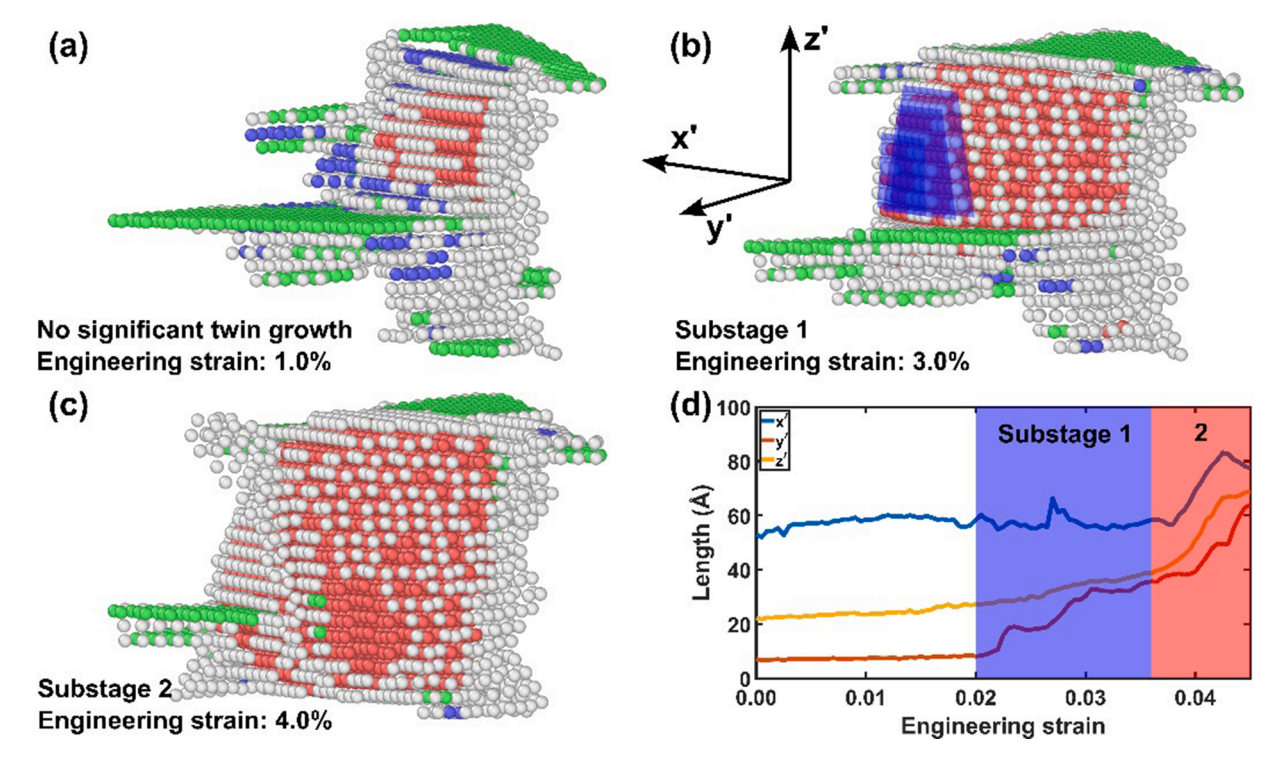


Fig. 7. Atomic snapshots showing the two substages after the twin nucleation. (a) for the stage where no significant twin growth occurs before the two substages, (b) for substage 1, and (c) for substage 2. Three adjacent transformed basal (B) planes in twin from prismatic (P) planes in matrix are highlighted in (b). (d) Twin lengths along the 3 axes in the local twin coordinate system, x', y' and z', are plotted as functions of engineering strain ε_{zz} . Approximate ranges of substage 1 and 2 are labeled, respectively, with substage 2 featuring a significant rise of z' length of the twin embryo.

density. The {10 $\overline{12}$ } deformation twin nucleates near the disconnection between two neighboring I $_1$ stacking faults, as in the case of 20% atom deletion, but with a lower number frequency due to the presence of only sparse I $_1$ stacking faults. These comparisons, as well as the parallel simulations that randomize the atom removal, validate that the most preferable twin nucleation site should be the disconnection between neighboring I $_1$ stacking faults, regardless of atom deletion percentage and the randomized structure of the stacking fault network.

4. Outlook and conclusions

This work describes and analyzes twin nucleation at disconnectiondense sites between two I1 stacking faults inside a complex defect network. By mimicking the dislocation formation in quenched materials with supersaturation of vacancies, a random defect network containing different types of dislocations, stacking faults, and disconnections is generated by annealing and quenching of a porous Mg in MD simulations, before a tensile deformation was applied. Our results indicate that the unique disconnection-dense sites are favorable for twin nucleation. These sites allow the P-B transformation to first occur on the plane spanned by the dislocation line of the disconnection and the c-axis of the matrix and later other parallel planes. This nucleation mechanism also results in the variant selection rule that sets the zone axis shared by the basal plane in the matrix and in the $\{10\overline{1}2\}$ twin to coincide with the dislocation line. Early-stage growth of the $\{10\overline{1}2\}$ twin after its nucleation has also been observed within an engineering strain of 5% along the c-axis. The twin growth can be categorized into two substages by the dominant growth direction. This study suggests a potential pure-shuffle pathway for twin nucleation in Mg, while the feasibility of the disconnection-rich structure in experiments and the energetics of the reported nucleation require further study.

Declaration of Competing Interest

The authors declare that they have no known competing financial interests or personal relationships that could have appeared to influence the work reported in this paper.

Acknowledgments

The authors acknowledge financial support from the National Science Foundation (NSF CMMI-1729829, NSF CMMI-1729887 and NSF CMMI-1723539). This work utilized the infrastructure for high-performance and high-throughput computing, research data storage and analysis, and scientific software tool integration built, operated, and updated by the Research Cyberinfrastructure Center (RCIC) at the University of California, Irvine (UCI). The RCIC provides cluster-based systems, application software, and scalable storage to directly support the UCI research community. The authors are also grateful to UCI for financial resources used in support of KY.

References

- J.F. Nie, K.S. Shin, Z.R. Zeng, Microstructure, deformation, and property of wrought magnesium alloys, Metall. Mater. Trans. A 51 (2020) 6045–6109, https://doi.org/10.1007/s11661-020-05974-z.
- [2] I.J. Beyerlein, L. Capolungo, P.E. Marshall, R.J. McCabe, C.N. Tomé, Statistical analyses of deformation twinning in magnesium, Philos. Mag. 90 (2010) 2161–2190, https://doi.org/10.1080/14786431003630835.
- [3] Q. Yu, J. Wang, Y. Jiang, R.J. McCabe, N. Li, C.N. Tomé, Twin–twin interactions in magnesium, Acta Mater. 77 (2014) 28–42, https://doi.org/10.1016/j. actamat.2014.05.030.
- [4] M. Arul Kumar, L. Capolungo, R.J. McCabe, C.N. Tomé, Characterizing the role of adjoining twins at grain boundaries in hexagonal close packed materials, Sci. Rep. 9 (2019), https://doi.org/10.1038/s41598-019-40615-5.
- [5] K. Dang, S. Wang, M. Gong, R.J. McCabe, J. Wang, L. Capolungo, Formation and stability of long basal-prismatic facets in Mg, Acta Mater. 185 (2020) 119–128, https://doi.org/10.1016/j.actamat.2019.11.070.

- [6] F. Wang, Y. Gu, R.J. McCabe, L. Capolungo, J.A. El-Awady, S.R. Agnew, < c + a >dislocations in {10-12} twins in Mg: a kinematic and energetic requirement, Acta Mater. 195 (2020) 13–24, https://doi.org/10.1016/j.actamat.2020.04.033.
- [7] L. Jiang, M. Gong, J. Wang, Z. Pan, X. Wang, D. Zhang, Y.M. Wang, J. Ciston, A. M. Minor, M. Xu, X. Pan, T.J. Rupert, S. Mahajan, E.J. Lavernia, I.J. Beyerlein, J. M. Schoenung, Visualization and validation of twin nucleation and early-stage growth in magnesium, Nat. Commun. 13 (2022) 20, https://doi.org/10.1038/s41467-021-27591-z.
- [8] J. Wang, J.P. Hirth, C.N. Tomé, (-1012) Twinning nucleation mechanisms in hexagonal-close-packed crystals, Acta Mater. 57 (2009) 5521–5530, https://doi. org/10.1016/j.actamat.2009.07.047.
- [9] K. Yaddanapudi, B. Leu, M.A. Kumar, X. Wang, J.M. Schoenung, E.J. Lavernia, T. J. Rupert, I.J. Beyerlein, S. Mahajan, Accommodation and formation of {-1012} twins in Mg-Y alloys, Acta Mater. 204 (2021), 116514, https://doi.org/10.1016/j.actamat.2020.116514.
- [10] M. Ghazisaeidi, W.A. Curtin, Analysis of dissociation of <c>and <c+ a>dislocations to nucleate (10-12) twins in Mg, Model. Simul. Mater. Sci. Eng. 21 (2013), 055007, https://doi.org/10.1088/0965-0393/21/5/055007.
- [11] R. Aghababaei, S.P. Joshi, Micromechanics of tensile twinning in magnesium gleaned from molecular dynamics simulations, Acta Mater. 69 (2014) 326–342, https://doi.org/10.1016/j.actamat.2014.01.014.
- [12] N. Thompson, D.J. Millard, Twin formation, in cadmium, Lond. Edinb. Dublin Philos. Mag. J. Sci. 43 (1952) 422–440, https://doi.org/10.1080/ 14786440408520175.
- [13] B.Y. Liu, J. Wang, B. Li, L. Lu, X.Y. Zhang, Z.W. Shan, J. Li, C.L. Jia, J. Sun, E. Ma, Twinning-like lattice reorientation without a crystallographic twinning plane, Nat. Commun. 5 (2014), https://doi.org/10.1038/ncomms4297.
- [14] Y. He, B. Li, C. Wang, S.X. Mao, Direct observation of dual-step twinning nucleation in hexagonal close-packed crystals, Nat. Commun. 11 (2020) 2483, https://doi.org/10.1038/s41467-020-16351-0.
- [15] J.W. Christian, S. Mahajan, Deformation twinning, Prog. Mater. Sci. 39 (1995) 1–157, https://doi.org/10.1016/0079-6425(94)00007-7.
- [16] H. El Kadiri, C.D. Barrett, M.A. Tschopp, The candidacy of shuffle and shear during compound twinning in hexagonal close-packed structures, Acta Mater 61 (2013) 7646–7659, https://doi.org/10.1016/j.actamat.2013.09.002.
- [17] J. Wang, S.K. Yadav, J.P. Hirth, C.N. Tomé, I.J. Beyerlein, Pure-shuffle nucleation of deformation twins in hexagonal-close-packed metals, Mater. Res. Lett. 1 (2013) 126–132, https://doi.org/10.1080/21663831.2013.792019.
- [18] I.J. Beyerlein, X. Zhang, A. Misra, Growth twins and deformation twins in metals, Annu. Rev. Mater. Res. 44 (2014) 329–363, https://doi.org/10.1146/annurevmatsci-070813-113304.

- [19] F. Sansoz, Atomistic processes controlling flow stress scaling during compression of nanoscale face-centered-cubic crystals, Acta Mater. 59 (2011) 3364–3372, https://doi.org/10.1016/j.actamat.2011.02.011.
- [20] S. Plimpton, Fast parallel algorithms for short-range molecular dynamics, J. Comput. Phys. 117 (1995) 1–19, https://doi.org/10.1006/jcph.1995.1039
- [21] D.Y. Sun, M.I. Mendelev, C.A. Becker, K. Kudin, T. Haxhimali, M. Asta, J.J. Hoyt, A. Karma, D.J. Srolovitz, Crystal-melt interfacial free energies in hcp metals: a molecular dynamics study of Mg, Phys. Rev. B 73 (2006), 024116, https://doi.org/ 10.1103/PhysRevB.73.024116.
- [22] D. Hull, D.J. Bacon, Introduction to Dislocations, 5 ed., Butterworth Heinemann, Elsevier, Amsterdam Heidelberg, 2011.
- [23] A. Stukowski, Visualization and analysis of atomistic simulation data with OVITOthe Open Visualization Tool, Model. Simul. Mater. Sci. Eng. 18 (2010), 015012, https://doi.org/10.1088/0965-0393/18/1/015012.
- [24] P. Tzanetakis, J. Hillairet, G. Revel, The formation energy of vacancies in aluminium and magnesium, Phys. Status Solidi B 75 (1976) 433–439, https://doi. org/10.1002/pssb.2220750205.
- [25] Y. Tang, J.A. El-Awady, Formation and slip of pyramidal dislocations in hexagonal close-packed magnesium single crystals, Acta Mater. 71 (2014) 319–332, https:// doi.org/10.1016/j.actamat.2014.03.022.
- [26] G. Agarwal, A.M. Dongare, Deformation twinning in polycrystalline Mg microstructures at high strain rates at the atomic scales, Sci. Rep. 9 (2019) 3550, https://doi.org/10.1038/s41598-019-39958-w.
- [27] A. Stukowski, V.V. Bulatov, A. Arsenlis, Automated identification and indexing of dislocations in crystal interfaces, Model. Simul. Mater. Sci. Eng. 20 (2012), 085007, https://doi.org/10.1088/0965-0393/20/8/085007.
- [28] D. Zhang, L. Jiang, J.M. Schoenung, S. Mahajan, E.J. Lavernia, TEM study on relationship between stacking faults and non-basal dislocations in Mg, Philos. Mag. 95 (2015) 3823–3844, https://doi.org/10.1080/14786435.2015.1100764.
- [29] C. He, Y. Zhang, C.Q. Liu, Y. Yue, H.W. Chen, J.F. Nie, Unexpected partial dislocations within stacking faults in a cold deformed Mg-Bi alloy, Acta Mater. 188 (2020) 328-343, https://doi.org/10.1016/j.actamat.2020.02.010.
- [30] P.M. Larsen, S. Schmidt, J. Schiøtz, Robust structural identification via polyhedral template matching, Model. Simul. Mater. Sci. Eng. 24 (2016), 055007, https://doi. org/10.1088/0965-0393/24/5/055007.
- [31] Y. Hu, V. Turlo, I.J. Beyerlein, S. Mahajan, E.J. Lavernia, J.M. Schoenung, T. J. Rupert, Embracing the Chaos: alloying adds stochasticity to twin embryo growth, Phys. Rev. Lett. 125 (2020), 205503, https://doi.org/10.1103/PhysRevLett.125.205503.
- [32] C. Pradalier, P.A. Juan, R.J. McCabe, L. Capolungo, A Graph theory-based automated twin recognition technique for electron backscatter diffraction analysis, Integr. Mater. Manuf. Innov. 7 (2018) 12–27, https://doi.org/10.1007/s40192-018-0106-y.